Reprinted with permission from the publisher.
*IEE Proceedings, Electric Power Applications.*
ISSN: 1350-2352
DOI:10.1049/ip-epa:20050550.
The original publication is available at www.theiet.org




Burakov, A., Arkkio, A. 2006. Low-order parametric force model for eccentric-rotor electrical machine with parallel connections in stator winding. *IEE Proceedings, Electric Power Applications*, Vol. 153, Issue 4, pp. 592-600.

# Low-order parametric force model for eccentric-rotor electrical machine with parallel connections in stator winding

A. Burakov and A. Arkkio

**Abstract:** A low-order parametric model, to accurately represent the eccentricity force acting in a salient-pole synchronous machine equipped with parallel stator windings, is proposed. The force model with parameters estimated from the numerical field calculation results exhibits an excellent performance in a wide whirling frequency range. Results presented also demonstrate the applicability of the model for the eccentricity force analysis in an induction machine. The proposed model provides an opportunity to combine the electromagnetic and mechanical analyses of electrical machine effectively.

## 1 Introduction

Nowadays, finite-element-based programs have become an everyday tool of the electrical machine designer. However, owing to the heavy computational burden, the calculations are still quite slow. Moreover, the complete analysis of an electrical machine, involving a coupled study of mechanical, electromagnetic and also thermal phenomena, would require a computational time beyond the practical limits. Therefore, there is a need for the development of simple parametric models that would be capable of quick yet accurate enough representation of one or more of the phenomena involved. Such models embedded into the main finite-element program could significantly reduce the computation time of a coupled problem. This paper puts forward a low-order parametric model for accurate representation of the eccentricity force acting in a salient-pole synchronous machine equipped with parallel stator windings.

An eccentric rotor motion (also called 'rotor whirling') occurs when the rotor axis of an electrical machine does not coincide with the axis of the stator bore but, instead, travels around the latter at a certain radius and angular speed (called whirling radius and whirling angular speed, respectively). Owing to manufacturing tolerances, wear of bearings, imperfect rotor mounting on its supports and other reasons, some degree of rotor eccentricity is always present. Rotor eccentricity generates the electromagnetic force (also known as unbalanced magnetic pull, UMP) that acts between the rotor and stator. The amplitude and direction of the force depend on the operating characteristics of the motor, whirling frequency and radius. Acting roughly in the direction of the shortest airgap, the UMP tries to further increase the eccentricity magnitude and may cause serious damage to the machine or even the whole drive.

The occurrence and effects of an eccentric rotor in electrical machines have been discussed for more than 100 years [1], and the beneficial effects of parallel windings in mitigating the resultant UMP have been discussed for almost as long [2]. Nowadays, it is a common practice for manufacturers to use parallel stator windings in motors since these are well known to reduce motor noise, vibration and UMP [3, 4]. Moreover, the parallel connections simplify the construction of the stator winding in large machines. Traditionally, analytical approaches were used to study the operation of an electrical machine with an eccentric rotor. In [3, 5], early attempts were made to account for the effects of parallel connections in the stator winding on the machine performance. More recent results of analytical research are presented in [6, 7]. Later, numerical methods have also been employed to study the UMP reduction by the parallel windings [8, 9].

Induction machines, being especially vulnerable to the rotor eccentricity due to the small airgap, have received a significant amount of attention from researchers [3, 4, 6–9]. Synchronous machines were considerably less popular as a research subject for several reasons: (*a*) the large airgap provided a weaker susceptibility to the rotor eccentricity; and (*b*) the salient-pole structure made the analysis of the machine more complicated.

The scope of almost every scientific paper written on the subject of rotor eccentricity is limited to the special cases of static eccentricity occurring when the rotor axis does not coincide with the stator bore axis, but remains stationary with respect to it; and/or dynamic eccentricity, which occurs when the rotor axis is eccentric and travels around the stator bore axis at an angular speed equal to the rotor mechanical speed. Only in [9] was the operation of an electrical machine in a wider range of whirling frequencies considered.

In this paper, a simple low-order parametric model to represent the eccentricity force acting in a salient-pole synchronous machine is developed and verified. The force model is designed for a machine accommodating parallel stator windings and is capable of accurately describing the eccentricity force in a wide whirling frequency range. The



*IEE Proceedings* online no. 20050550

doi:10.1049/ip-epa:20050550

Paper first received 28th December 2005 and in revised form 10th March 2006

The authors are with Helsinki University of Technology, Laboratory of Electromechanics, PO Box 3000, FIN-02015 HUT, Finland

E-mail: Andrej.Burakov@tkk.fi

methods used in this work involve the magnetic field analysis based on the classical permeance harmonic theory presented by Früchtenicht *et al.* [10] and the findings of Arkkio *et al.* [11] to build up a force model. The impulse method developed by Tenhunen *et al.* [12] is employed in the numerical calculations to efficiently obtain the data needed for the estimation of force model parameters. The force model with estimated parameters shows an excellent performance in a wide whirling frequency range. The proposed force model has the following advantages:

- it allows simple, quick and accurate calculation of the electromagnetic force at a desired whirling frequency value or in a certain range of whirling frequencies
- the same model parameters can be directly used at different values of whirling radius and whirling frequency
- the model offers an attractive opportunity to be integrated into the mechanical analysis to study the electromechanical interactions in electrical machines
- the model performs very accurately when applied to synchronous and induction machines with different number of parallel stator windings; no changes are needed in the model expression.

The limitations of the force model are:

- the necessity to re-estimate the force model parameters every time the operating point (supply voltage, load torque etc.) of a machine is changed
- applicability to the electrical machines that only have parallel stator windings and are not equipped with a rotor cage.

## 2 Methods of analysis

In this work, a salient-pole synchronous machine operating in the steady state was studied. Therefore, the fundamental component of the magnetic flux density was assumed to be constant, unaffected by the rotor eccentricity. Only the cylindrical circular rotor whirling was considered, meaning that the rotor axis when travelling at a circular orbit around the stator bore axis remained always parallel to it. Despite the rotor saliency, the machine was analysed in the stator reference frame without resorting to the classical two-axis approach. Instead, a vector representation was used, which allowed for a considerably improved clarity, conciseness and simplicity of the resultant expressions.

The cross-section view of the machine studied is shown in Fig. 1. The stator and rotor axes were assumed to be perpendicular to the plane of the Figure and the magnetic field in the core region was assumed to be two-dimensional and parallel to this plane. Although, the field winding magnetomotive force (MMF) in a salient-pole synchronous machine is constant within the angular length of a rotor pole, hereafter, we use the sinusoidal distribution of the MMF. This assumption simplifies the magnetic field analysis and has almost no effect on the spatial distribution of the resultant magnetic flux density in the airgap. More details on this simplification are given in Section 2.1.

The machine studied is equipped with four parallel stator windings connected in such a way that the neighbouring pole windings are in series and the opposite pole windings are in parallel. Motors incorporating this kind of stator winding have been reported to run more quietly than those with neighbouring pole windings in parallel and the opposite pole windings in series [8].

This study is focused on the effects the parallel stator windings have on the electromagnetic force generated by the rotor eccentricity. Therefore, the damper winding (rotor cage) was not considered in the analytical part. During numerical calculations, the influence of the damper winding was eliminated by using 'air' as the material of the winding. The parallel paths of the field winding, which are expected to have UMP reduction effects similar to those of the damper winding, are also not considered here.

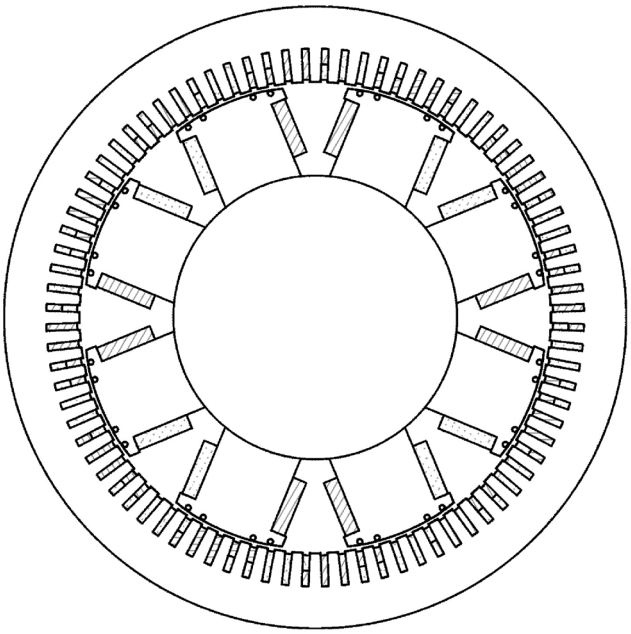

**Fig. 1** *Cross-sectional view of simulated machine*

The original rotor of the synchronous machine was slotted. For simulation purposes, material of the rotor cage was changed from copper to air (equivalent to removing the copper from the rotor slots). By doing this, the permeance harmonics (called slot harmonics) associated with rotor slotting remained virtually unaffected. But of course, the MMF harmonics (called step harmonics) produced by the rotor cage were eliminated. As a result, removing the copper from the rotor slots affected the magnitude of the magnetic field harmonics associated with the rotor slotting, but it did not introduce any new harmonics.

### 2.1 Magnetomotive forces

The resultant MMF of the machine studied consists of MMFs produced by the armature (stator) and field (rotor) windings.

The field winding is concentrated on the rotor poles. Therefore, the MMF spectrum of this winding contains several harmonics. For an eight-pole machine studied, five most prominent field winding MMF components and their values relative to the fundamental MMF component are given in Table 1.

As seen, the fundamental component of the field winding MMF is preponderant. As for the stator winding MMF,

**Table 1: Content of field winding MMF spectrum**

| Harmonic (number of pole-pairs) | Relative magnitude |
|---|---|
| 4 | 1 |
| 12 | 0.199 |
| 20 | 0.016 |
| 28 | 0.030 |
| 36 | 0.02 |

the supremacy of the fundamental component is expected to be even greater because of the more even distribution of the winding conductors along the machine circumference. Therefore, in the following, only the fundamental MMF component is considered. This simplification was also used in [13], where the general model for the analysis of a salient-pole machine as well as for a non-salient-pole machine was developed.

The field winding rotates with the rotor, and thus its MMF can be expressed as

$$F_{\mathrm{f}}(\varphi) = \mathrm{Re}\left\{\left(\frac{N_{\mathrm{f}}}{2p} i_{\mathrm{f}}\right) \mathrm{e}^{\mathrm{j}(p\varphi-\omega_1 t)}\right\} = \mathrm{Re}\{F_{\mathrm{f},p}\mathrm{e}^{\mathrm{j}(p\varphi-\omega_1 t)}\} = \mathrm{Re}\{\underline{F}_{\mathrm{f},p}\} \quad (1)$$

where $p$ is the number of pole-pairs and the corresponding wave-number; $N_{\mathrm{f}}$ is the number of field winding turns in series; $i_{\mathrm{f}}$ is field winding current; $\omega_1 = p\Omega_{\mathrm{m}}$ is the angular frequency of the stator supply; $\Omega_{\mathrm{m}}$ is the mechanical angular velocity of the rotor; $\varphi$ is the angular coordinate; $t$ denotes time; bar underlining a quantity means that the corresponding quantity is complex-valued.

In the parallel stator windings, currents induced by the magnetic flux harmonics can circulate. Those having non-zero winding factors would also generate the corresponding MMF harmonics:

$$F_{\mathrm{s}}(\varphi) = \sum_{m=1}^{N_1} \mathrm{Re}\left\{\left(\frac{3}{2}\frac{N_{\mathrm{se},m}}{2p} i_m\right) \mathrm{e}^{\mathrm{j}(m\varphi-\omega_m t)}\right\} = \sum_{m=1}^{N_1} \mathrm{Re}\{F_m \mathrm{e}^{\mathrm{j}(m\varphi-\omega_m t)}\} \quad (2)$$

where $m$ is the wave-number of the MMF harmonic; $N_1$ is the highest harmonic of the stator MMF, $N_{\mathrm{se},m} = 4k_{\mathrm{sw},m}N_{\mathrm{s}}/\pi$ is the equivalent number of the stator winding turns in series for the $m$th stator current harmonic; $k_{\mathrm{sw},m}$ is the winding factor for the corresponding stator current harmonic; $N_{\mathrm{s}}$ is the number of stator winding turns in series; and $i_m$ is the stator current harmonic, which causes the MMF harmonic with wave-number $m$. Note that a current harmonic induced by a magnetic flux harmonic passing through a single parallel circuit of the stator winding contains in itself only the time variation. But, when interacting with currents of the same frequency in other parallel windings, it causes the MMF harmonic, which has a spatial distribution.

The net MMF is the sum of the field and stator winding MMFs:

$$F(\varphi) = \mathrm{Re}\left\{(F_{\mathrm{f},p} + F_p)\mathrm{e}^{\mathrm{j}(p\varphi-\omega_1 t)} + \sum_{\substack{m=1,\\ m\neq p}}^{N_1} F_m \mathrm{e}^{\mathrm{j}(m\varphi-\omega_m t)}\right\} \quad (3)$$

As already mentioned, the MMF of the field winding is not sinusoidally distributed but rather constant over the rotor pole. On the other hand, the airgap length over the pole-shoe is varying and so is the airgap permeance. This is done for the purpose of achieving a sinusoidal distribution of the magnetic flux density produced by the field winding. In this work, we have used a sinusoidal distribution of the field winding MMF and a constant airgap (if no eccentricity is present) instead of actual constant MMF and varying airgap length. It can be shown that both approaches provide very similar distributions of the magnetic flux density in the airgap.

## 2.2 Airgap permeance

In [14], it was shown that the circumferencial airgap variation in a salient-pole synchronous machine can be expressed as

$$\delta(\varphi) = \mathrm{Re}\left\{\frac{\delta_0}{\left|\cos\left(\frac{\pi}{\tau}\varphi\right)\right|} \mathrm{e}^{-\mathrm{j}2\omega_1 t}\right\} \quad (4)$$

where $\delta_0$ is the smallest airgap between the rotor pole shoe and the stator surface (on the pole axis); $\tau$ is the pole pitch $\tau = \frac{\pi}{p}$; and $|\,|$ denotes the absolute value.

Equation (4) can also be written as

$$\delta(\varphi) = \mathrm{Re}\left\{\frac{\delta_0}{|\cos(p\varphi)|} \mathrm{e}^{-\mathrm{j}2\omega_1 t}\right\} \quad (5)$$

Cylindrical rotor whirling causes an additional term in the airgap expression:

$$\delta(\varphi) = \mathrm{Re}\left\{\frac{\delta_0}{|\cos(p\varphi)|} \mathrm{e}^{-\mathrm{j}2\omega_1 t} + \delta_{\mathrm{ecc}} \mathrm{e}^{\mathrm{j}(\varphi-\omega_{\mathrm{ecc}}t+\varphi_{\mathrm{ecc.0}})}\right\} \quad (6)$$

where $\delta_{\mathrm{ecc}}$ is whirling radius; $\omega_{\mathrm{ecc}}$ is whirling angular speed; and $\varphi_{\mathrm{ecc.0}}$ is the initial phase angle of the rotor eccentricity.

Airgap permeance is calculated taking the inverse of the airgap

$$\lambda(\varphi) = \frac{\mu_0}{\delta(\varphi)} \quad (7)$$

where $\mu_0$ is permeability of a free space. Substituting (6) into (7) results in a Fourier series in which the most prominent components have wave-numbers 0, 1 and $2p$ (see also Fig. 2, where the rotor eccentricity value was 20% of the airgap):

$$\lambda(\varphi) = \frac{\mu_0}{\delta_0}\left(1 + \frac{1}{\delta_0}\mathrm{Re}\{\delta_{\mathrm{ps}}\mathrm{e}^{\mathrm{j}(2p\varphi-2\omega_1 t)}\} + \frac{1}{\delta_0}\mathrm{Re}\{\delta_{\mathrm{ecc}}\mathrm{e}^{\mathrm{j}(\varphi-\omega_{\mathrm{ecc}}t+\varphi_{\mathrm{ecc.0}})}\}\right) \quad (8)$$

where the term $\delta_{\mathrm{ps}}\mathrm{e}^{\mathrm{j}(2p\varphi-2\omega_1 t)}$ is due to the rotor saliency.

## 2.3 Magnetic flux density

The magnetic flux density in the airgap is obtained as a product of MMF and permeance:

$$B(\varphi) = F(\varphi)\lambda(\varphi) \quad (9)$$

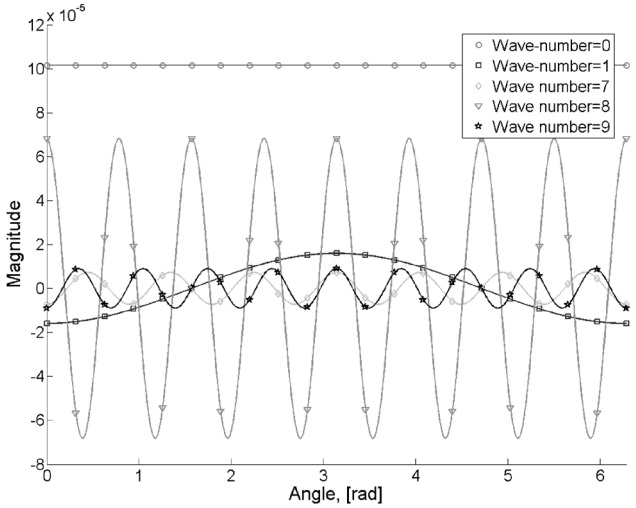


**Fig. 2** *Airgap permeance waves for eight-pole machine*

Substituting (3) and (8) into (9) yields

$$
\begin{aligned}
B(\varphi) = \frac{\mu_0}{\delta_0}\mathrm{Re}\Bigg\{ & \Bigg[(F_{\mathrm{f},p}+F_p)\mathrm{e}^{-\mathrm{j}\omega_1 t}+\frac{\delta_{\mathrm{ps}}}{2\delta_0}\big((F_{\mathrm{f},p}+F_p)\mathrm{e}^{-\mathrm{j}\omega_1 t} \\
& + F_{3p}\mathrm{e}^{-\mathrm{j}(\omega_{3p}-2\omega_1)t}\big)+\frac{\delta_{\mathrm{ecc}}}{2\delta_0}\big(F_{p-1}\mathrm{e}^{-\mathrm{j}((\omega_{p-1}+\omega_{\mathrm{ecc}})t-\varphi_{\mathrm{ecc},0})} \\
& + F_{p+1}\mathrm{e}^{-\mathrm{j}((\omega_{p+1}-\omega_{\mathrm{ecc}})t+\varphi_{\mathrm{ecc},0})}\big)\Bigg]\mathrm{e}^{\mathrm{j}p\varphi} \\
& + \Bigg[F_{p-1}\mathrm{e}^{-\mathrm{j}\omega_{p-1}t}+\frac{\delta_{\mathrm{ecc}}}{2\delta_0}(F_{\mathrm{f},p}+F_p)\mathrm{e}^{-\mathrm{j}((\omega_1-\omega_{\mathrm{ecc}})t+\varphi_{\mathrm{ecc},0})} \\
& + \frac{\delta_{\mathrm{ps}}}{2\delta_0}\big(F_{p+1}\mathrm{e}^{\mathrm{j}(\omega_{p+1}-2\omega_1)t}+F_{3p-1}\mathrm{e}^{-\mathrm{j}(\omega_{3p-1}-2\omega_1)t}\big)\Bigg]\mathrm{e}^{\mathrm{j}(p-1)\varphi} \\
& + \Bigg[F_{p+1}\mathrm{e}^{-\mathrm{j}\omega_{p+1}t}+\frac{\delta_{\mathrm{ecc}}}{2\delta_0}(F_{\mathrm{f},p}+F_p)\mathrm{e}^{-\mathrm{j}((\omega_1+\omega_{\mathrm{ecc}})t-\varphi_{\mathrm{ecc},0})} \\
& + \frac{\delta_{\mathrm{ps}}}{2\delta_0}\big(F_{p-1}\mathrm{e}^{\mathrm{j}(\omega_{p-1}-2\omega_1)t}+F_{3p+1}\mathrm{e}^{-\mathrm{j}(\omega_{3p+1}-2\omega_1)t}\big)\Bigg]\mathrm{e}^{\mathrm{j}(p+1)\varphi} \\
& + \sum_{\substack{m=1,\\ m\neq p;\,p\pm1}}^{N_1} F_m\mathrm{e}^{\mathrm{j}(m\varphi-\omega_m t)}+\frac{\delta_{\mathrm{ecc}}}{2\delta_0}\Bigg(F_{p-1}\mathrm{e}^{\mathrm{j}((p-2)\varphi-(\omega_{p-1}-\omega_{\mathrm{ecc}})t-\varphi_{\mathrm{ecc},0})} \\
& + F_{p+1}\mathrm{e}^{\mathrm{j}((p+2)\varphi-(\omega_{p+1}+\omega_{\mathrm{ecc}})t+\varphi_{\mathrm{ecc},0})} \\
& + \sum_{\substack{m=1,\\ m\neq p;\,p\pm1}}^{N_1} F_m\mathrm{e}^{\mathrm{j}((m\pm1)\varphi-(\omega_m\pm\omega_{\mathrm{ecc}})t\pm\varphi_{\mathrm{ecc},0})}\Bigg) \\
& + \frac{\delta_{\mathrm{ps}}}{2\delta_0}\Bigg((F_{\mathrm{f},p}+F_p)\mathrm{e}^{\mathrm{j}(3p\varphi-3\omega_1 t)}+F_{p-1}\mathrm{e}^{\mathrm{j}((3p-1)\varphi-(\omega_{p-1}+2\omega_1)t)} \\
& + F_{p+1}\mathrm{e}^{\mathrm{j}((3p+1)\varphi-(\omega_{p+1}+2\omega_1)t)}+F_{3p}\mathrm{e}^{\mathrm{j}(5p\varphi-(\omega_{3p}+2\omega_1)t)} \\
& + F_{3p-1}\mathrm{e}^{\mathrm{j}((5p-1)\varphi-(\omega_{3p-1}+2\omega_1)t)}+F_{3p+1}\mathrm{e}^{\mathrm{j}((5p+1)\varphi-(\omega_{3p+1}+2\omega_1)t)} \\
& + \sum_{\substack{m=1,\\ m\neq p;\,p\pm1;3p;3p\pm1}}^{N_1} F_m\mathrm{e}^{\mathrm{j}((m\pm2p)\varphi-(\omega_m\pm2\omega_1)t)}\Bigg)\Bigg\}
\end{aligned}
\tag{10}
$$

Note that, in (10), the $p-1$ magnetic flux density harmonic can be produced by the interaction of the $p+1$ MMF harmonic with the permeance wave due to the rotor saliency (note the term $\frac{\delta_{\mathrm{ps}}}{2\delta_0}F_{p+1}\mathrm{e}^{-\mathrm{j}((p-1)\varphi+(\omega_{p+1}-2\omega_1)t)}$). Similarly, the product of $p-1$ MMF harmonic and the same permeance wave can generate a magnetic flux density harmonic with wave-number $p+1$ (term $\frac{\delta_{\mathrm{ps}}}{2\delta_0}F_{p-1}\mathrm{e}^{-\mathrm{j}((p+1)\varphi+(\omega_{p-1}-2\omega_1)t)}$). Although these constituents of the $p\pm1$ magnetic flux density terms are expected to be small and are neglected hereafter, they show that there can be a coupling between the two magnetic flux density harmonics, commonly known as eccentricity harmonics.

Rotor eccentricity mainly generates the magnetic flux density terms having wave-numbers $p$ and $p\pm1$. Therefore, by taking into account only the strongest magnetic flux density components, (10) can be reduced to

$$
\begin{aligned}
B(\varphi) = \frac{\mu_0}{\delta_0}\mathrm{Re}\Bigg\{ & \Bigg[(F_{\mathrm{f},p}+F_p)\mathrm{e}^{-\mathrm{j}\omega_1 t}+\frac{\delta_{\mathrm{ps}}}{2\delta_0}(F_{\mathrm{f},p}+F_p)\mathrm{e}^{-\mathrm{j}\omega_1 t}\Bigg]\mathrm{e}^{\mathrm{j}p\varphi} \\
& + \Bigg[F_{p-1}\mathrm{e}^{-\mathrm{j}\omega_{p-1}t}+\frac{\delta_{\mathrm{ecc}}}{2\delta_0}(F_{\mathrm{f},p}+F_p)\mathrm{e}^{-\mathrm{j}((\omega_1-\omega_{\mathrm{ecc}})t+\varphi_{\mathrm{ecc},0})}\Bigg]\mathrm{e}^{\mathrm{j}(p-1)\varphi} \\
& + \Bigg[F_{p+1}\mathrm{e}^{-\mathrm{j}\omega_{p+1}t}+\frac{\delta_{\mathrm{ecc}}}{2\delta_0}(F_{\mathrm{f},p}+F_p)\mathrm{e}^{-\mathrm{j}((\omega_1+\omega_{\mathrm{ecc}})t-\varphi_{\mathrm{ecc},0})}\Bigg]\mathrm{e}^{\mathrm{j}(p+1)\varphi}\Bigg\}
\end{aligned}
\tag{11}
$$

Equation (11) can be rewritten as

$$
B(\varphi) = \mathrm{Re}\{\underline{B}_p\mathrm{e}^{\mathrm{j}p\varphi}+\underline{B}_{p-1}\mathrm{e}^{\mathrm{j}(p-1)\varphi}+\underline{B}_{p+1}\mathrm{e}^{\mathrm{j}(p+1)\varphi}\} \tag{12}
$$

where the shortening notations are

$$
\begin{aligned}
\underline{B}_p &= \frac{\mu_0}{\delta_0}\left[(F_{\mathrm{f},p}+F_p)\mathrm{e}^{-\mathrm{j}\omega_1 t}+\frac{\delta_{\mathrm{ps}}(F_{\mathrm{f},p}+F_p)}{2\delta_0}\mathrm{e}^{-\mathrm{j}\omega_1 t}\right] \\
\underline{B}_{p-1} &= \frac{\mu_0}{\delta_0}\left[\frac{\delta_{\mathrm{ecc}}(F_{\mathrm{f},p}+F_p)}{2\delta_0}\mathrm{e}^{-\mathrm{j}((\omega_1-\omega_{\mathrm{ecc}})t+\varphi_{\mathrm{ecc},0})}+\underline{F}_{p-1}\right] \\
\underline{B}_{p+1} &= \frac{\mu_0}{\delta_0}\left[\frac{\delta_{\mathrm{ecc}}(F_{\mathrm{f},p}+F_p)}{2\delta_0}\mathrm{e}^{-\mathrm{j}((\omega_1+\omega_{\mathrm{ecc}})t-\varphi_{\mathrm{ecc},0})}+\underline{F}_{p+1}\right]
\end{aligned}
\tag{13}
$$

Equation (13) can also be written using current harmonics:

$$
\begin{aligned}
\underline{B}_p &= \frac{\mu_0}{2p\delta_0}\left[N_{\mathrm{f}}i_{\mathrm{f}}+\frac{3}{2}N_{\mathrm{se},p}i_p+\frac{\delta_{\mathrm{ps}}}{2\delta_0}\left(N_{\mathrm{f}}i_{\mathrm{f}}+\frac{3}{2}N_{\mathrm{se},p}i_p\right)\right]\mathrm{e}^{-\mathrm{j}\omega_1 t} \\
&= (B_{p,1}+B_{p,2})\mathrm{e}^{-\mathrm{j}\omega_1 t} \\
\underline{B}_{p-1} &= \frac{\delta_{\mathrm{ecc}}}{2\delta_0}B_{p,1}\mathrm{e}^{-\mathrm{j}((\omega_1-\omega_{\mathrm{ecc}})t+\varphi_{\mathrm{ecc},0})}+\frac{\mu_0}{\delta_0}k_{p-1}\underline{i}_{p-1} \\
\underline{B}_{p+1} &= \frac{\delta_{\mathrm{ecc}}}{2\delta_0}B_{p,1}\mathrm{e}^{-\mathrm{j}((\omega_1+\omega_{\mathrm{ecc}})t-\varphi_{\mathrm{ecc},0})}+\frac{\mu_0}{\delta_0}k_{p+1}\underline{i}_{p+1}
\end{aligned}
\tag{14}
$$

where $B_{p,1}$ is caused by the interaction of the fundamental MMF components and constant permeance; $B_{p,2}$ is the result of interaction of the fundamental MMF components with permeance wave due to the rotor saliency; and $k_{p\pm1}$ are dimensionless coupling factors.

## 2.4 Magnetic flux through stator winding

Magnetic flux waves with wave-numbers $p\pm1$ through the stator winding can be written as

$$
\begin{aligned}
\underline{\Psi}_{p-1} &= L_{\mathrm{s},p-1}\left(\frac{\delta_{\mathrm{ecc}}k_{p-1}}{2\mu_0}B_{p,1}\mathrm{e}^{-\mathrm{j}((\omega_1-\omega_{\mathrm{ecc}})t+\varphi_{\mathrm{ecc},0})}+\underline{i}_{p-1}\right) \\
\underline{\Psi}_{p+1} &= L_{\mathrm{s},p+1}\left(\frac{\delta_{\mathrm{ecc}}k_{p+1}}{2\mu_0}B_{p,1}\mathrm{e}^{-\mathrm{j}((\omega_1+\omega_{\mathrm{ecc}})t-\varphi_{\mathrm{ecc},0})}+\underline{i}_{p+1}\right)
\end{aligned}
\tag{15}
$$

where $L_{\mathrm{s},p\pm1}$ are the self-inductances of the stator winding for the corresponding magnetic flux density waves. According to [10], the self-inductances are defined as $L_{\mathrm{s},p\pm1}=\mu_0\frac{p_{\mathrm{pp}}d_{\mathrm{s}}l_{\mathrm{e}}N^2K_{\mathrm{w},p\pm1}}{2\delta_{\mathrm{e}}}$, where $p_{\mathrm{pp}}$ is the pitch of the parallel path in the stator winding (radians), $d_{\mathrm{s}}$ is the inner diameter of the stator bore, $l_{\mathrm{e}}$ is the equivalent axial length of the machine, $N$ is the number of turns in the parallel path of the stator winding, $K_{\mathrm{w},p\pm1}$ is the corresponding winding factor and $\delta_{\mathrm{e}}$ is the equivalent airgap including the effect of slotting.

## 2.5 Voltage equations

As mentioned above, the stator connection type where the neighbouring pole windings are connected in series and the opposite pole windings are in parallel is considered in this work. The analysis is also suitable for machines having as many parallel stator windings as there are poles. Flux linkages through the parallel paths of such windings have the same magnitude but are phase-shifted with respect to each other. For a magnetic flux harmonic having

wave-number $v$, the phase-shift between the neighbouring parallel windings is given as

$$\gamma_v = \frac{2\pi v}{N_{\mathrm{pp}}} \tag{16}$$

where $N_{\mathrm{pp}}$ is the number of parallel paths in the stator winding.

Now it can be readily verified that $p\pm1$ magnetic flux harmonics through the parallel stator windings are phase-shifted by an angle $2\pi/N_{\mathrm{pp}}$ and their vector sum gives zero. Therefore, assuming the impedances of the parallel windings to be identical, the stator winding can be studied as a symmetric balanced $N_{\mathrm{pp}}$-phase circuit. Thus, the voltage equation for $p\pm1$ harmonics in the stator winding is

$$\left(R_{p\pm1} + L_{\sigma,p\pm1}\frac{\mathrm{d}}{\mathrm{d}t}\right)\underline{i}_{p\pm1,n} + \frac{\mathrm{d}\underline{\Psi}_{p\pm1,n}}{\mathrm{d}t} = 0 \tag{17}$$

where $\underline{i}_{p\pm1,n}$ is the $(p\pm1)$th current harmonic flowing in the $n$th parallel path of the stator winding; $\underline{\Psi}_{p\pm1,n}$ is $(p\pm1)$th harmonic of the magnetic flux linkage through the $n$th parallel path, $L_{\sigma,p\pm1}$ is the stator leakage inductance for a corresponding harmonic, and $R_{p\pm1}$ is the resistance of the parallel path for a corresponding harmonic. The voltage $\underline{U}_{\mathrm{s}}$ connected to the stator terminals is assumed to consist of the fundamental component only. The path through the stator terminals for non-fundamental current harmonics can be considered as a short circuit (the impedance of the grid, to which the machine is connected is usually quite small).

By inserting flux linkage equations into the corresponding voltage equations, expressions for the stator current harmonics are obtained:

$$\begin{aligned}
&\left(R_{p-1} + L_{p-1}\frac{\mathrm{d}}{\mathrm{d}t}\right)\underline{i}_{p-1} - \mathrm{j}(\omega_1 - \omega_{\mathrm{ecc}}) \\
&\quad\times \frac{\delta_{\mathrm{ecc}} k_{p-1} L_{\mathrm{s},p-1}}{2\mu_0} B_{p,1}\mathrm{e}^{-\mathrm{j}((\omega_1-\omega_{\mathrm{ecc}})t+\varphi_{\mathrm{ecc.0}})} = 0 \\
&\left(R_{p+1} + L_{p+1}\frac{\mathrm{d}}{\mathrm{d}t}\right)\underline{i}_{p+1} - \mathrm{j}(\omega_1 + \omega_{\mathrm{ecc}}) \\
&\quad\times \frac{\delta_{\mathrm{ecc}} k_{p+1} L_{\mathrm{s},p+1}}{2\mu_0} B_{p,1}\mathrm{e}^{-\mathrm{j}((\omega_1+\omega_{\mathrm{ecc}})t-\varphi_{\mathrm{ecc.0}})} = 0
\end{aligned} \tag{18}$$

where $L_{p\pm1} = L_{\mathrm{s},p\pm1} + L_{\sigma,p\pm1}$ are the total inductances of the stator winding for the corresponding magnetic flux density waves.

From (18), $p\pm1$ stator current harmonics can be solved:

$$\begin{aligned}
\underline{i}_{p-1} &= \frac{k_{p-1} L_{\mathrm{s},p-1} B_{p,1}\delta_{\mathrm{ecc}}}{2\mu_0 L_{p-1}}\left[-1 + \frac{1}{1 - \mathrm{j}(\omega_1 - \omega_{\mathrm{ecc}})\dfrac{L_{p-1}}{R_{p-1}}}\right] \\
&\quad\times \mathrm{e}^{-\mathrm{j}((\omega_1-\omega_{\mathrm{ecc}})t+\varphi_{\mathrm{ecc.0}})} \\
\underline{i}_{p+1} &= \frac{k_{p+1} L_{\mathrm{s},p+1} B_{p,1}\delta_{\mathrm{ecc}}}{2\mu_0 L_{p+1}}\left[-1 + \frac{1}{1 - \mathrm{j}(\omega_1 + \omega_{\mathrm{ecc}})\dfrac{L_{p+1}}{R_{p+1}}}\right] \\
&\quad\times \mathrm{e}^{-\mathrm{j}((\omega_1+\omega_{\mathrm{ecc}})t-\varphi_{\mathrm{ecc.0}})}
\end{aligned} \tag{19}$$

Since this study is only concerned with the steady-state operation of an electrical machine, the transient current components are not shown in (19).

## 2.6 Total electromagnetic force on rotor

To calculate the electromagnetic force acting on the rotor, Maxwell's stress is applied:

$$\sigma = \frac{1}{2\mu_0}[B(\varphi)]^2 = \frac{1}{2\mu_0}\left[\sum_{v=0}^{\infty}\mathrm{Re}\{\underline{B}_v(\varphi)\mathrm{e}^{\mathrm{j}v\varphi}\}\right]^2 \tag{20}$$

The total electromagnetic force is obtained by integrating Maxwell's stress over the whole circumferential length of a machine:

$$\underline{F}_{\mathrm{e}} = \frac{d_{\mathrm{r}} l_{\mathrm{e}}}{2}\int_0^{2\pi}\sigma(\varphi)\mathrm{e}^{\mathrm{j}\varphi}\mathrm{d}\varphi \tag{21}$$

where $d_{\mathrm{r}}$ is the outer diameter of the rotor, and $l_{\mathrm{e}}$ is the equivalent axial length of the machine.

Assuming that the force on the rotor is generated due to the product of two magnetic flux density harmonics it can be written as

$$\underline{F}_{\mathrm{e}} = \frac{d_{\mathrm{r}} l_{\mathrm{e}}}{2\mu_0}\int_0^{2\pi}(\underline{B}_v\underline{B}_w^*\mathrm{e}^{\mathrm{j}(v-w+1)\varphi} + \underline{B}_v^*\underline{B}_w\mathrm{e}^{-\mathrm{j}(v-w-1)\varphi})\mathrm{d}\varphi \tag{22}$$

Thus, the net force can only be produced by the magnetic flux density components with wave-numbers satisfying the condition $v - w = \pm1$.

Rotor eccentricity mainly causes the magnetic flux components of orders $p$, $p-1$ and $p+1$ (see (14)). Therefore, the electromagnetic force due to the eccentric rotor can be expressed as

$$\begin{aligned}
\underline{F}_{\mathrm{e}} = &\frac{\pi d_{\mathrm{r}} l_{\mathrm{e}}}{4\mu_0\delta_0}(B_{p,1} + B_{p,2})\big(B_{p,1}\delta_{\mathrm{ecc}}\mathrm{e}^{\mathrm{j}(\omega_{\mathrm{ecc}}t-\varphi_{\mathrm{ecc.0}})} \\
&+ \mu_0 k_{p-1}\underline{i}_{p-1}\mathrm{e}^{\mathrm{j}\omega_1 t} + \mu_0 k_{p+1}\underline{i}_{p+1}^*\mathrm{e}^{-\mathrm{j}\omega_1 t}\big)
\end{aligned} \tag{23}$$

Substituting the stator current harmonics from (19) into (23) yields

$$\begin{aligned}
\underline{F}_{\mathrm{e}} = &\frac{\pi d_{\mathrm{r}} l_{\mathrm{e}}}{4\mu_0\delta_0}B_{p,1}(B_{p,1} + B_{p,2}) \\
&\times\left[1 + \frac{k_{p-1}^2 L_{\mathrm{s},p-1}}{2L_{p-1}}\left(-1 + \frac{1}{1 - \mathrm{j}(\omega_1 - \omega_{\mathrm{ecc}})\dfrac{L_{p-1}}{R_{p-1}}}\right)\right. \\
&\left.+\frac{k_{p+1}^2 L_{\mathrm{s},p+1}}{2L_{p+1}}\left(-1 + \frac{1}{1 + \mathrm{j}(\omega_1 + \omega_{\mathrm{ecc}})\dfrac{L_{p+1}}{R_{p+1}}}\right)\right]\delta_{\mathrm{ecc}}\mathrm{e}^{\mathrm{j}(\omega_{\mathrm{ecc}}t-\varphi_{\mathrm{ecc.0}})}
\end{aligned} \tag{24}$$

The parametric form of (24) is

$$\begin{aligned}
\frac{\underline{F}_{\mathrm{e}}}{\delta_{\mathrm{ecc}}\mathrm{e}^{\mathrm{j}(\omega_{\mathrm{ecc}}t-\varphi_{\mathrm{ecc.0}})}} = K(\mathrm{j}\omega_{\mathrm{ecc}}) &= r_0 + \frac{r_{p-1,1}}{r_{p-1,2} + \mathrm{j}(\omega_{\mathrm{ecc}} - \omega_1)} \\
&+ \frac{r_{p+1,1}}{r_{p+1,2} + \mathrm{j}(\omega_{\mathrm{ecc}} + \omega_1)}
\end{aligned} \tag{25}$$

where $K(\mathrm{j}\omega_{\mathrm{ecc}})$ is the frequency response function (FRF) of the electromagnetic force, the '$r$' symbols represent real-valued parameters, and subscript '0' defines the FRF component independent of the whirling frequency, whereas subscripts '$p\pm1$' label the FRF components related to the corresponding eccentricity harmonics of the magnetic field.

Equation (25) is a parametric model representing the electromagnetic force on the whirling rotor as a function of

whirling radius and whirling angular speed. The model parameters can be estimated using numerical simulation results. Thus, the model accounts for the effects of iron core saturation, slotting and equalising currents in the parallel stator windings because all these are considered in the simulation.

### 2.7 Numerical calculation

The numerical calculation of the magnetic field was based on the transient time-stepping finite-element analysis (FEA) [15]. The magnetic field and circuit equations were discretised and solved together as a system of equations. The time dependence of the variables was modelled by the Crank-Nicholson method. The forces were calculated at each time step using a method developed by Coulomb [16].

Several simplifications were made in order to keep the amount of computation to a reasonable level. The magnetic field in the core region was assumed to be two-dimensional. The laminated iron core was treated as a non-conducting magnetically nonlinear medium, and the nonlinearity was modelled by a single-valued magnetisation curve.

The impulse method [12] was implemented in the FEA, which allowed the FRF of the force, in the whole studied whirling frequency range ($[-100, 100]$ Hz), to be obtained using the results of a single numerical simulation, thus significantly reducing the computation time.

## 3 Results

To estimate the force model parameters, the aforementioned salient-pole synchronous machine was simulated using the FEA. The main parameters of the machine are given in Table 2.

**Table 2: Main parameters of simulated synchronous machine**

| Parameter | Value |
|---|---|
| Number of pole-pairs | 4 |
| Frequency of voltage supplied to stator winding, Hz | 50 |
| Stator winding supply voltage, V | 6300 |
| Field winding supply voltage, V | 150 |
| Stator winding connection | star |
| Apparent power, kVA | 8400 |
| Power factor | 0.83 cap. |

The machine was operated in a steady-state generator mode and connected to a constant line voltage. The mechanical angular velocity of the rotor was kept constant. The machine had four parallel stator windings and was simulated without the rotor cage.

To demonstrate how strongly the UMP is influenced by the parallel connections in the stator winding, the FRFs were calculated for a machine with four parallel stator windings and for the same machine with a series-connected stator winding. The two corresponding FRFs of the force are shown in Fig. 3. The complex-valued FRFs in Fig. 3 are resolved into real and imaginary parts, which correspond to radial and tangential force components, respectively.

Force model parameters were calculated from the FEA results employing the genetic-algorithm-based estimation program. The estimated force model parameters for a

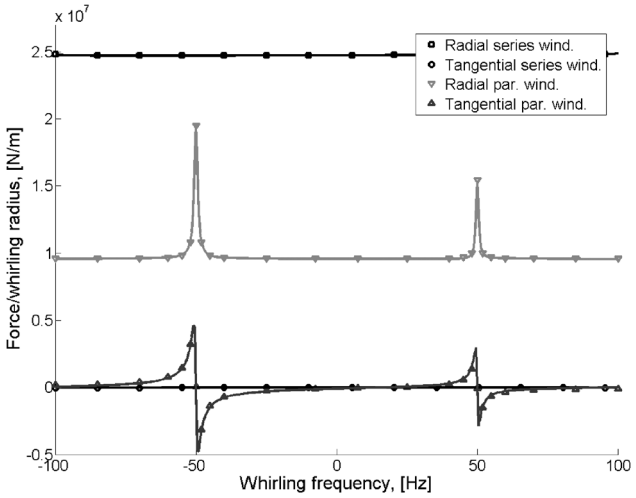


**Fig. 3** *FRF of force calculated using FEA*
Case *a*: four parallel stator windings
Case *b*: series-connected stator winding

**Table 3: Estimated force model parameters for synchronous machine**

| Parameter | Unit | Value |
|---|---|---|
| $r_0$ | $\frac{N}{m}$ | $9.6 \times 10^6$ |
| $r_{p-1,1}$ | $\frac{N_s}{m}$ | $1.96 \times 10^7$ |
| $r_{p-1,2}$ | $s^{-1}$ | 3.35 |
| $r_{p+1,1}$ | $\frac{N_s}{m}$ | $4.57 \times 10^7$ |
| $r_{p+1,2}$ | $s^{-1}$ | 4.62 |

machine with four parallel stator windings are given in Table 3.

To evaluate the performance of the presented force model, these parameters were substituted into the force model expression (25). By doing this, the estimated FRF of the force was obtained. Comparison of the estimated FRF against the original FRF from the FEA is shown in Fig. 4.

The performance of the parametric force model applied to an induction machine was also studied. For simulation purposes, the material of the rotor cage was changed from aluminium to air, which is equivalent to the removal of the rotor bars. Although, the use of such an induction machine in real life is not practical, this application example helped

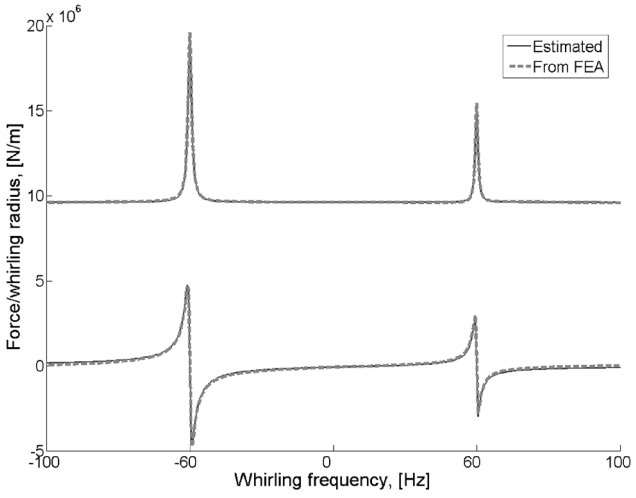


**Fig. 4** *Comparison of the estimated FRF against FRF from FEA*

us to assess the generalisation capability of the force model developed. Table 4 gives the main parameters of the second test motor. Table 5 gives the estimated force model parameters for this machine, when the stator has four parallel windings. Figure 5 shows the performance of the force model with the estimated parameters. Figure 6 shows a typical trajectory of the electromagnetic force vector in the same induction machine but with two parallel stator windings. Table 6 gives the force model parameters estimated for the case of two parallel stator windings. The performance of the force model in this case is shown in Fig. 7. Note that in this analysis, the effects of the rotor cage on the electromagnetic forces were neglected.

**Table 4: Main parameters of induction machine**

| Parameter | Value |
|---|---|
| Number of pole-pairs | 2 |
| Rated frequency, Hz | 50 |
| Rated voltage, V | 380 |
| Rated power, kW | 15 |
| Connection | delta |
| Skew of the rotor slots | 0 |
| Number of parallel stator windings | 4(2) |

**Table 5: Estimated force model parameters for induction machine with four parallel stator windings**

| Parameter | Unit | Value |
|---|---|---|
| $r_0$ | $\frac{N}{m}$ | $3.66 \times 10^6$ |
| $r_{p-1,1}$ | $\frac{N_s}{m}$ | $2.99 \times 10^7$ |
| $r_{p-1,2}$ | $s^{-1}$ | 5.45 |
| $r_{p+1,1}$ | $\frac{N_s}{m}$ | $2.85 \times 10^8$ |
| $r_{p+1,2}$ | $s^{-1}$ | $3.29 \times 10$ |

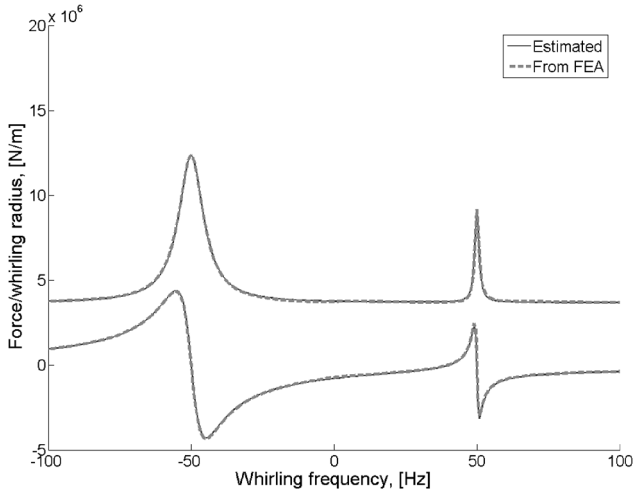


**Fig. 5** *Performance evaluation of force model applied to induction machine with four parallel stator windings*

## 4 Discussion

The FRFs of the force obtained from the FEA (Fig. 3) were resolved into two orthogonal components: the radial one—acting in the direction of the shortest airgap; and the tangential one, which is perpendicular to the radial one. The radial and tangential force components rotate together with the point of the shortest airgap. The tangential component of the electromagnetic force due to the rotor eccentricity must be distinguished from the tangential force responsible for the machine's torque generation during the normal operation. In the context of this paper, the term 'tangential component' refers only to the electromagnetic force produced due to the rotor eccentricity. According to the results of our FEA calculations, rotor eccentricity has only a minor effect on the tangential stresses responsible for the torque production.

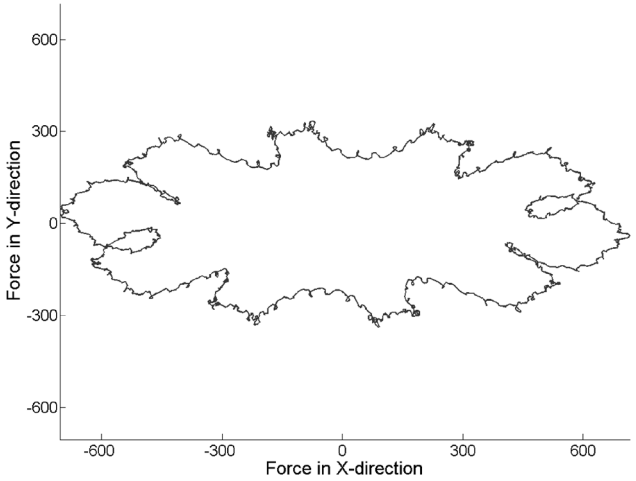


**Fig. 6** *Typical trajectory of electromagnetic force vector in induction machine with two parallel stator windings*

**Table 6: Estimated force model parameters for induction machine with two parallel stator windings**

| Parameter | Unit | Value |
|---|---|---|
| $r_0$ | $\frac{N}{m}$ | $9.86 \times 10^6$ |
| $r_{p-1,1}$ | $\frac{N_s}{m}$ | $1.83 \times 10^7$ |
| $r_{p-1,2}$ | $s^{-1}$ | 5.58 |
| $r_{p+1,1}$ | $\frac{N_s}{m}$ | $5.83 \times 10^7$ |
| $r_{p+1,2}$ | $s^{-1}$ | $1.83 \times 10$ |

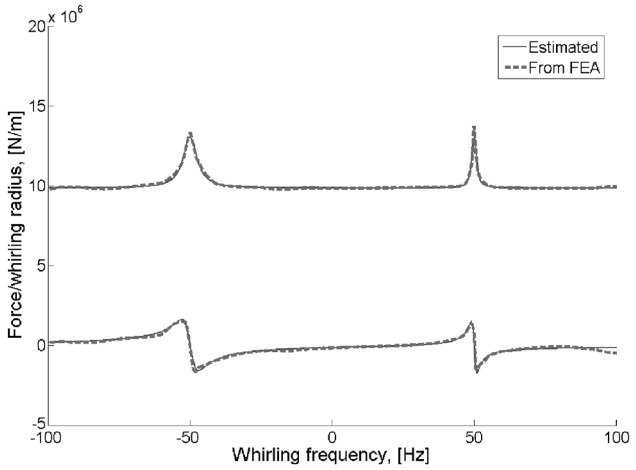


**Fig. 7** *Performance evaluation of force model applied to induction machine with two parallel stator windings*

In [12], it is mentioned that the frequency of the eccentricity force is often smaller than that of the fundamental field. As this work is focused on the electromagnetic forces created by rotor eccentricity, the whirling frequency range of interest was chosen to be $[-100, 100]$ Hz. A negative whirling frequency implies that the point of the shortest airgap travels in the direction opposite to that of the mechanical rotor motion.

Comparing the FRFs shown on Fig. 3 it is seen that the parallel stator windings provide a significant reduction of the radial eccentricity force component. The average reduction of the radial UMP in the whirling frequency range $[-100, 100]$ Hz is over 60%. On the other hand, the parallel stator windings increase the tangential component of the eccentricity force, which, in the case of series-connected stator winding, is negligible. However, since the radial force component is considerably stronger than the tangential one, the mean reduction of the absolute UMP value in the studied whirling frequency range is still over 60%.

According to (19), the $p \pm 1$ stator current harmonics vanish at the whirling frequencies of $\mp 50$ Hz, respectively. Therefore, the parallel stator windings do not damp the corresponding magnetic flux density harmonics and, as a result, the radial UMP component has two sharp peaks, at these particular whirling frequency values. At $-50$ Hz, where the $p+1$ stator current harmonic is zero, the radial force component has a maximum value. Thus, it can be concluded that the $p+1$ magnetic field harmonic plays a more important role in the UMP generation than the $p-1$ harmonic. At $-50$ Hz, the UMP damping by the parallel stator windings is at its minimum value (about 20%). This observation is also confirmed by examining the estimated force model parameters given in Table 3. As seen, the parameter $r_{p+1,1}$, which defines the amplitude of the FRF peak at $-50$ Hz, has more than two times greater value than the parameter $r_{p-1,1}$, which is responsible for the FRF peak at 50 Hz. Tables 5 and 6 show that, in the case of induction machine, the ratio between the force model parameters $r_{p+1,1}$ and $r_{p-1,1}$ is yet greater.

Figure 4 shows that the FRF of the force, obtained by substituting the estimated parameters into the force model expression (25), agrees very well with the FRF calculated by the FEA. The maximum error between the absolute values of the two FRFs is 1.6%, whereas the average error in the whole studied whirling frequency range is 0.7%. Thus, a conclusion can be made that, in case of a salient-pole synchronous machine, the results produced by the developed force model match very well the results from FEA. This excellent model performance is exhibited throughout the whole studied whirling frequency range.

Inspecting (24), it is seen that the only term pertinent to the rotor saliency is the constituent of the fundamental magnetic flux density $B_{p,2}$. Thus, eliminating the influence of the rotor saliency would not affect the expression of the parametric force model, (25). Therefore, the force model was also applied to the induction machine, having parallel stator windings and operating without the rotor cage. Although, the use of such an induction machine in real life is not practical, this application example helped in the assessment of the generalisation capability of the force model developed. Figure 5 also clearly demonstrates that, in the case of induction machine with four parallel stator windings, the FRF of the force provided by the developed force model corresponds very well to the FRF of the force calculated by the FEA.

The induction machine equipped with two parallel stator windings was also studied. It also has to be mentioned that, in this case, the impulse method was not capable of providing accurate results and, therefore, a conventional forced whirling method was used. In this approach, the rotor axis was forced to move along a circular orbit at a constant angular velocity in the time-stepping FEA. More details on this method can be obtained from [11]. The FEA results revealed that, unlike the rotor axis, the eccentricity force vector has an elliptic trajectory (see Fig. 6). It means that two parallel stator windings cause uneven UMP damping on the orthogonal axes. Therefore, it was decided to draw the FRF curves using the average force values. Figure 7 shows that the force model developed also performed very well in the case of an induction machine with two parallel stator windings. Larger discrepancies between the FRF from the FEA and the estimated one (maximum error approx. 7%, average error 0.86%) are due to the averaging used. Comparing the results shown in Figs. 5 and 7 it is clearly seen that the machine equipped with four parallel stator windings provides a significantly more effective attenuation of the radial UMP component than the machine with two parallel stator windings. But it is interesting to observe that the tangential component of the eccentricity force in the machine with four parallel stator windings is expected to be stronger than in the machine with two parallel stator windings.

The force model presented has several advantages:

1. Simple, quick and accurate calculation of the electromagnetic force: by substituting the estimated parameters into the model expression, the force at a certain whirling frequency value or in a certain range of whirling frequencies can be calculated in a matter of seconds.

2. Applicability at different whirling radius and whirling frequency values: when creating the force model, it was assumed that the force is a linear function of the rotor displacement. Since the FRF represents the force per whirling radius as a function of whirling frequency, the same model parameters can be used at different values of rotor eccentricity within the whole particular whirling frequency range. Again, there is no need to carry out the time-consuming finite-element calculations. For more information related to the UMP linearity the reader is referred to [17].

3. An attractive opportunity to study the electromechanical interactions in electrical machines: the parametric force model integrated into mechanical analysis of the machine would only marginally increase the computational burden of the calculations without loss of accuracy of the final results.

4. As indicated by the application examples the force model, developed to be primarily used with synchronous machines, performs also very successfully when applied to induction machines; no changes are needed in the model expression. Moreover, the model proved to be accurate when used with electrical machines having different numbers of parallel stator windings.

The presented force model has also several limitations. First, the estimated set of force model parameters corresponds to a certain operating point of a machine. Once the operating point (supply voltage, load torque etc.) is changed the FRF of the force must be recalculated and a new set of parameters established. Slot harmonics are considered as one of the main reasons for the electromagnetic force dependence on the load point. These have a very small whirling-frequency dependence in the range considered but can vary significantly owing to the load

changes. Secondly, the developed force model is only valid for an electrical machine, which has parallel stator windings and has no damper winding.

As said before, there were no new magnetic field harmonics introduced into the airgap of the simulated machines owing to the replacement of the original rotor cage materials with air. The force model developed accounts for the effects of iron core saturation, slotting and equalising currents in the parallel stator windings.

It is worth mentioning that the force model developed in this work is very simple, containing only five real-valued parameters, which all have a physical meaning.

Synchronous machines are often equipped with both: the parallel stator windings and the damper winding. In addition, the field winding may also have parallel paths. These machines are expected to have smoother operation than those having only one of the aforementioned UMP damping mechanisms. The electromagnetic analysis of such machines issues new challenges because the damping effects produced by the rotor and stator windings cannot be considered separately, but rather in a coupled manner. This is a topic for future research.

## 5 Conclusions

The influence of the parallel stator windings on the UMP in a salient-pole synchronous machine with eccentric rotor has been studied. Based on the theory elaborated and results acquired, a simple parametric force model has been developed and verified. The model parameters were estimated from the results of FEA, where the effects of slotting, iron core saturation and equalising currents in the parallel stator windings were all taken into account. The force model with estimated parameters shows an excellent performance in a wide whirling frequency range.

The proposed force model has the following advantages:

1. it allows simple, quick and accurate calculation of the electromagnetic force at a desired whirling frequency value or in a certain range of whirling frequencies

2. the same model parameters can be directly used at different values of whirling radius and whirling frequency

3. the model offers an attractive opportunity to be integrated into the mechanical analysis to study the electromechanical interactions in electrical machines

4. the model performs very accurately when applied to synchronous and induction machines with different numbers of parallel stator windings; no changes are needed in the model expression.

The limitations of the force model are:

1. the necessity to re-estimate the force model parameters every time the operating point (supply voltage, load torque etc.) of a machine is changed

2. applicability to electrical machines that only have parallel stator windings and are not equipped with a rotor cage.

## 6 Acknowledgment

The authors thank Prof. T. Jokinen for advice concerning the theoretical part of the work.

## 7 References

1 Fisher-Hinnen, J.: 'Dynamo design' (Van Nostrand, 1899)
2 Hellmund, R.E.: 'Series versus parallel windings for a.c. motors', *Electr. World*, 1907, (49) pp. 388–389
3 Krondl, M.: 'Self excited radial vibrations of the rotor of induction machines with parallel paths in the winding', *Bull. Assoc. Suisse Electr.*, 1956, **47**, pp. 581–588
4 Ellison, A.J., and Yang, S.J.: 'Effects of rotor eccentricity on acoustic noise from induction machines', *Proc. IEE*, 1977, **118**, (1), pp. 174–183
5 Robinson, R.C.: 'The calculation of unbalanced magnetic pull in synchronous and induction motors', *AIEE Trans.*, 1943, **62**, pp. 620–624
6 Berman, M.: 'On the reduction of magnetic pull in induction motors with off-centre rotor'. Conf. Record of the IEEE Industry Applications Society Annual Meeting, October 1993, Vol. 1, pp. 343–350
7 Dorrell, D.G., and Smith, A.C.: 'Calculation of UMP in induction motors with series or parallel winding connections', *IEEE Trans. Energy Convers.*, 1994, **9**, (2), pp. 304–310
8 DeBortoli, M.J., Salon, S.J., Burow, D.W., and Slavik, C.J.: 'Effects of rotor eccentricity and parallel windings on induction machine behaviour: a study using finite element analysis', *IEEE Trans. Magn.*, 1993, **29**, (2), pp. 1676–1682
9 Tenhunen, A., Holopainen, T.P., and Arkkio, A.: 'Effects of equalizing currents on electromagnetic forces of whirling cage rotor'. Proc. IEMDC'03, June 2003, Vol. 1, pp. 257–263
10 Früchtenicht, J., Jordan, H., and Seinsch, H.O.: 'Exzentrizitätsfelder als Ursache von Lafinstabilitäten bei Asynchronmaschinen. Teil I und II', *Arch. Elektrotech.*, 1982, **65**, pp. 271–292
11 Arkkio, A., Antila, M., Pokki, K., Simon, A., and Lantto, E.: 'Electromagnetic force on a whirling cage rotor', *IEE Proc. Electr. Power Appl.*, 2000, **147**, pp. 353–360
12 Tenhunen, A., Holopainen, T.P., and Arkkio, A.: 'Impulse method to calculate the frequency response of the electromagnetic forces on whirling cage rotors', *IEE Proc. Electr. Power Appl.*, 2003, **150**, (6), pp. 752–756
13 Shi, C., and Li, M.: 'A general model of synchronous machine for its steady-state performance analysis', *IEEE Trans. Energy Convers.*, 1990, **5**, (3), pp. 531–537
14 Richter, R.: 'Elektrische maschinen' (Zweiter Band, Verlag Birkhäuser, Basel/Stuttgart, 1953), p. 707
15 Arkkio, A.: 'Analysis of induction motors based on the numerical solution of the magnetic field and circuit equations', *Acta Polytechn. Scand. Electr. Eng. Ser.*, 1987, p. 97
16 Coulomb, J.L.: 'A methodology for the determination of global electromechanical quantities from a finite element analysis and its application to the evaluation of magnetic forces, torques and stiffness', *IEEE Trans. Magn.*, 1983, **19**, (6), pp. 2514–2519
17 Tenhunen, A., Holopainen, T.P., and Arkkio, A.: 'Spatial linearity of unbalanced magnetic pull in induction motors during eccentric rotor motions', *COMPEL—Int. J. Comput. Math. Electr. Electron. Eng.*, 2003, **22**, (4), pp. 862–876